# Numerical analysis of new lock enhanced integral geocell reinforced sand beds

Juan Hou, Meng Xi Zhang & Hao Li
*Department of Civil Engineering, Shanghai University, China*

ABSTRACT: The paper describes the numerical analysis results of strip footings supported on new lock enhanced integral geocell reinforced sand beds. The 3-D finite element package ABAQUS was used to perform more realistic three-dimensional, nonlinear finite element analyses. The interface between soil and reinforcement is modeled by the contact pair option in ABAQUS. The numerical model was validated with the experimental studies and the results are found to be in good agreement with each other. The validated numerical model was used to study the influence of the geocells on the performance of the reinforced foundation. It was found that new lock enhanced integral geocell can decrease settlement and increase bearing capacity of foundation. Both vertical and horizontal displacement and the stress distribution of the soil foundation were studied. It was found that the geocells reinforcement layer can decrease both displacement and stress. The vertical confinement of geocells is due to the friction between the infill material and the geocell wall and restrains the soil from moving outside. The geocell-reinforced base can thus provide lateral and vertical confinement, tensioned membrane effect, and wider stress distribution which result in better performance.

*Keywords: lock enhanced integral geocell, FEM, mechanism, numerical model, stress, displacement*

## 1 INTRODUCTION

The technique of soil reinforcing using geocell is widely used in geotechnical engineering such as foundations, embankments, highways, retaining walls, and slope protections. The most of the commercial geocells available nowadays are made with ultrasonically welded high-density polyethylene (HDPE) strips. Many experimental and field studies reported the beneficial aspects of HDPE geocell (Zhou and Wen 2008, Dash 2012). Yuu et al. (2008) summarized that the key benefits of geocell used as base reinforcement are to confine fill inside the three-dimensional polymeric honeycomb cells to reduce its lateral movement. Despite the effectiveness of the geocell system, some researchers found that the majority of the HPDE geocell failures occur in the form of either excessive wall deformation or joint rupture (Han et al. 2007, Hedge and Sitharam 2014a). Therefore alternatives are needed to improve geocell stiffness and joint strength. Recently, lock enhanced integral geocell (LEIG) was carried out in China. As shown in Fig.1, the LEIG is constructed by insert U shape pins into predrill slits in polypropylene geocell strips and then expanded to 3-dimensional square box. Because the ensemble of overall strips and stiffness of U shape pins, the LEIG geocell is characterized by higher stiffness and higher joint strength relative to geocell made from HDPE. According to standard Q/DK02, the tension strength of a polypropylene strip is more than 16kN/m. The fracture strain is less than 15%. The shear strength of a U shape pin is no less than 6kN. The joint strength is no less than strip strength. Successful projects have proven that the use of these LEIG geocells can be mechanized construction and offer faster, cheaper, sustainable solutions to many complex geotechnical problems. However, as a new type of geothyntics, a considerable gap exists between the applications and the theories for the mechanisms of LEIG geocell-reinforced foundations. Han et al. (2014) made an attempt to evaluate the overall performance of LEIG geocell layers in improving the bearing capacity through model tests. The effect of geometry of the geocell such as the pocket opening size, height, and depth of placement of the geocell layer was discussed. However, the mecha-

nisms for footings on LEIG geocell reinforced soils haven not yet been well understood because the mechanisms is difficult to be completely visualized in experimental tests. This lack of studies in the subject area was the motive behind the planning of the present research work.

Numerical modeling is the most favored technique to find the failure mechanism (Lee and Eun 2009, Bathurst et al. 2009). When emphasis on studying the influence of reinforcement on the overall performance of the bed, it would be preferable to work with equivalent two-dimensional models (Mehdipour et al. 2013, Latha, 2014). This approach is very simple and can represent the three-dimensional nature of the geocell with improved strength and stiffness values of soil.

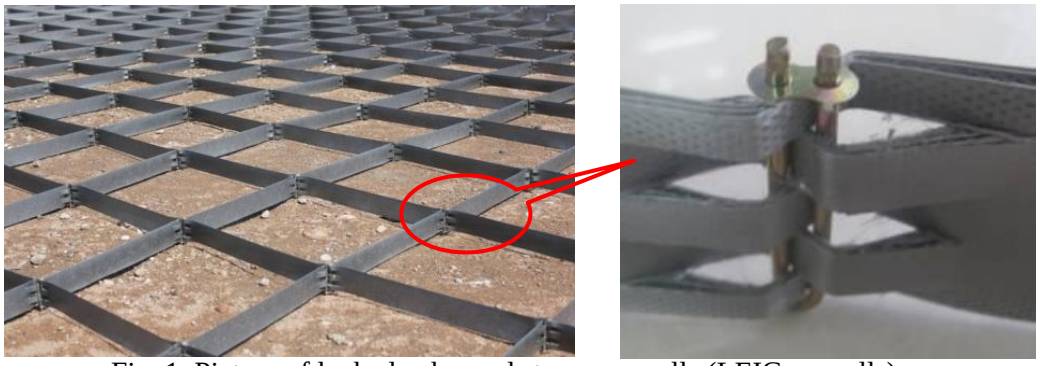

Fig. 1. Picture of locked enhanced strong geocells (LEIG geocells)

While in-depth investigation such as load transfers mechanisms between three-dimensional geocell and soil is needed, a three-dimensional numerical method is a more effective way. Han et al. (2007) studied a geocell-reinforced gravel base over soft subgrade under a circular footing. The HPDE honeycomb geocells were modeled using the linearly elastic structural (geogrid) elements provided by the FLAC$^{3D}$ software. Through investigating the stress distribution on geocell, they stated that it is important to have sufficient strength at the welding joints of the HPDE geocell. Hegde and Sitharam (2014) assumed the cylindrical shape of the geocell and discussed the joint strength and the wall deformation characteristics of a single cell when it is subjected to uniaxial compression. Leshchinsky and Ling (2013) modeled the multiple cell geocell reinforced base using ABAQUS and studied the effects of geocell confinement on strength and deformation behavior of gravel.

In this study, unreinforced and LEIG geocell-reinforced bases were modeled using a three-dimensional numerical model to improve the understanding of mechanisms of LEIG geocell-reinforced bases. The finite element package ABAQUS$^{3D}$ is used. For validate the numerical results convenience, the dimension of the model was kept equal to the dimension of the test bed used in the experiments. The properties of LEIG geocell similar to the experimental study were also used in the numerical model. The variety of geomaterials such as sand and LEIG geocell is modeled by different material models and elements in order to simulate the real case scenario.

Exact 3-dimensional square box of LEIG geocell was modeled by 8-node, quadrilateral, first-order interpolation, stress/displacement continuum shell element with reduced integration (SC8R). The soil was modeled by 8-node brick element with reduced integration (C3D8R). The interface elements were used to accurately model the joints and the interfaces between two materials. The displacement and the stress distribution of the soil foundation were studied. The tensile stress, the friction and the contact stress distribution on the surface of geocell were also investigated.

## 2 NUMERICAL MODEL

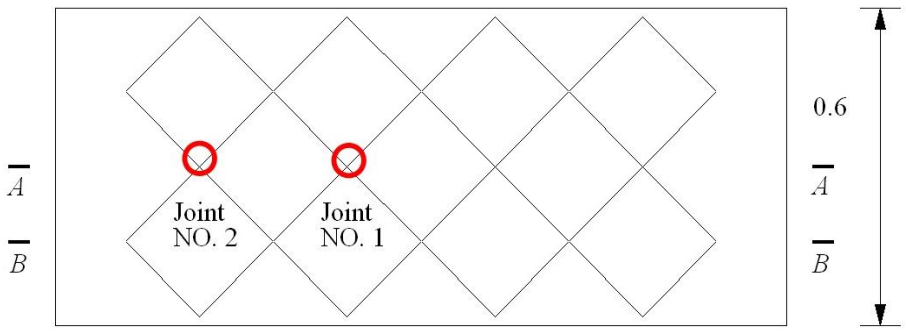


Fig. 2. The schematic of numerical model (unit: m)

Fig. 2 shows the schematic representation of the numerical model. The inner dimensions of the test tank are 0.6m (width) ×1.4m (length) ×1.1m (depth). The depth of soil bed is 0.65m. A rigid steel square plate 0.3m (width) ×0.03m (thick) was used as the square footing in the tests. Footing was placed at the top of the bed at a pre-determined alignment. The LEIG geocell were provided by Jiangsu Yizheng Geotechnical Composite Co., Ltd. The pocket size with a single cell diameter of d=20 cm and height h = 5 cm was modeled. The geocell is placed at a depth of 0.33*B* (*B* is the width of footing). For convenience discuss later in part 4, the depth (z), the horizontal distance (x), and the settlement (s) was normalized by footing width *B* in the paper. The cross section "A" and "B", the joint number 1 and 2 are also marked on schematic plan. The soil and geocell properties which were kept the same as that of the experiments are as shown in Table 1 and Table 2, respectively.

Table 1 Soil properties.

| Density (kg/m$^3$) | *E* (kPa) | $\mu$ | $\phi$ (°) | c (kPa) | constitutive relations |
|---|---|---|---|---|---|
| 1810 | $3\times10^3$ | 0.42 | 35 | 0 | Drucker-Prager model |

Table 2 Geocell properties.

| Density(kg/m$^3$) | *E* (kPa) | $\mu$ | Tension strength (Mpa) | constitutive relations |
|---|---|---|---|---|
| 1800 | $3\times10^6$ | 0.30 | 244 | linear elastic |

The finite element package ABAQUS$^{3D}$ was used to perform three-dimensional, nonlinear finite element analyses. The soil can be characterized employing the Drucker-Prager model, which are the most widely used material models for simulating soil behavior in ABAQUS. The geocell can be modeled as an elastic material because the maximum strain of the geocell strip is less than 5% during the tests (Han et al. 2014).

The soil was meshed using the most widely used C3D8R (8-node brick element with reduced integration) for simulating soil. The geocell was meshed using SC8R (8-node, quadrilateral, first-order interpolation, stress/displacement continuum solid element with reduced integration). A typical model used for the numerical simulations is shown in Fig. 4. The number of soil elements of unreinforced sand and geocell reinforced sand bed is 4368 and 7803, respectively. The number of geocell elements is 468. The interface between soil and reinforcement is modeled by the contact pair option in ABAQUS. This option allows sticking, sliding or separation to occur between the contact elements, obeying the Mohr-Coulomb criterion. The surface of the geocell was selected to be a master surface and the surface of soil was selected to be the slave surface in contact pair. When surfaces are in contact, they usually transmit shear as well as normal forces across their interface. Thus, the analysis may need to take frictional forces which resist the relative sliding of the surfaces into account. The friction model characterizes the frictional behavior between the surfaces using a coefficient of friction. Based on the tension test results, the coefficient of friction is 0.8.

The displacement along the bottom boundary (which represents tank bottom) was restrained in both horizontal as well as vertical directions. The side boundaries (which represent tank side) were restrained only in the horizontal direction, such that the displacements were allowed to occur in the vertical direction. The forces applied at the area of 30cm×30cm in the center of tank. Analyses were carried out under 100 kPa steps of static pressure from 100 to 600 kPa.

## 3 RESULTS AND DISCUSSIONS

### 3.1 *Pressure-settlement Response*

The given model has been validated with a single cell (Hou et al. 2015). Contour of contact stress along both height and length direction and friction distribution on the inside/outside surface of a single cell has been studied. Hence, the model was extended to multiple cells and aims to analysis the whole affection of the geocell on foundation. Fig. 3 represents the comparison of the bearing pressure-settlement curve obtained from experimental and numerical studies. The numerically predicted responses show a very good match with the experimental ones. A maximum error of prediction not exceeding 5% was obtained. Thus, the results from the finite element models can be used to investigate the mechanism of reinforced foundation.

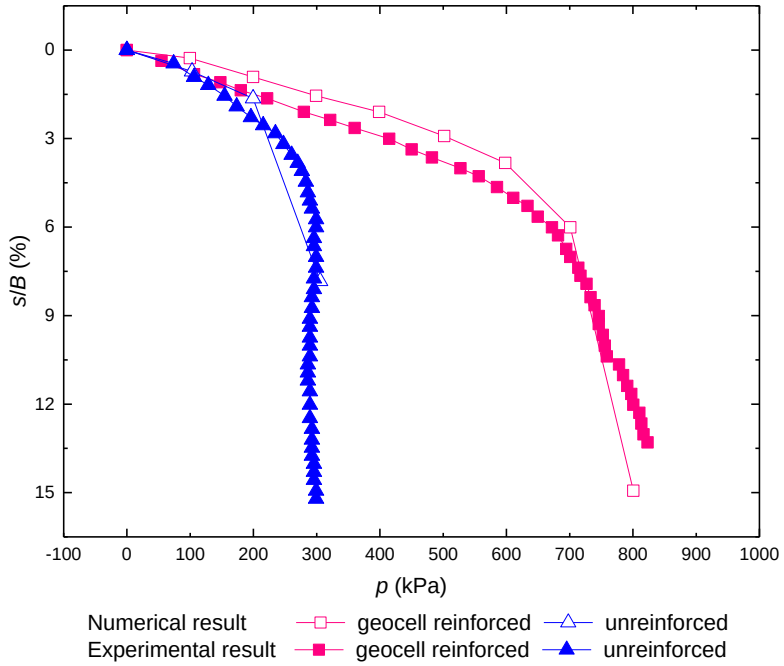


Fig. 3. Bearing pressure-settlement behavior

### 3.2 *The displacement of the soil foundation*

Fig. 4 shows the vertical displacement contours of "A" cross section as shown in Fig. 2 for different cases at the pressure of 300kPa (ultimate bearing capacity of the unreinforced bed). It can be seen clearly that settlement in reinforced situation with geocell layer decreases obviously comparing to the unreinforced one. The maximum reduction about 80% can be found at the center of footing. Uniform distribution of the contours indicates the uniform vertical displacement of the footing in the geocell reinforced case. Furthermore, it can be found that in case of geocells, the vertical displacement is transferred to a relatively shallow depth as compared to the unreinforced one. For both cases i.e., reinforced and unreinforced, the vertical displacement contour values reduce gradually with increasing the depth of the test bed. For increase in depth beyond 1.2*B* and 1.8*B* in reinforced and unreinforced foundation respectively, the vertical displacement is marginal. These observations also revealed that the boundary distances did not influence the results as deformations were contained within the boundaries.

Fig. 5 shows the horizontal displacement contours of "A" cross section for different cases. The observations revealed that the boundary distances did not influence the results as deformations were contained within the boundaries. It is evident from the observed results that the geocell reinforced case yields the more uniform reduction of horizontal displacement peaks than the unreinforced one. The geocell occupies the depth from 0.3*B* to 0.5*B* below the footing and marked by dash line in the Fig. 5b. Comparing Fig. 5a to 5b, it can be seen that the remarkable constraint due to the geocell is happened at the top of the joint of NO.1 (x=0.47*B*, marked by circle). From Fig. 5c, it can be seen that the horizontal displacement curve of reinforced case is completely different from unreinforced case. A sudden decrease at the joint of geocell can be found in reinforced case while gently decrease and disappear can be found in unreinforced case. The maximum horizontal displacement is about 50% as compared to the unreinforced sand bed. The confinement effect gradually decreases as the distance away from the center of footing increases. At the joint of NO.2 (x=1.4*B*), the horizontal displacement tends to be zero. It indicates that the length of geocell layer has an optimum value, beyond which further improvements were marginal. It also indicates that the geocell should be located under the footing. Fig. 5d represents the horizontal displacement curves for different type of reinforcements to investigate the effect of the depth of reinforced zone on the sand beds. It can be seen that the horizontal displacement curve of reinforced case is completely different from unreinforced case in the reinforced fill zone (depth<0.5*B*). On the contrast, the horizontal displacement curves tend to be of little difference by increasing depth from 0.5*B* to 2*B* (out the reinforced fill zone). It

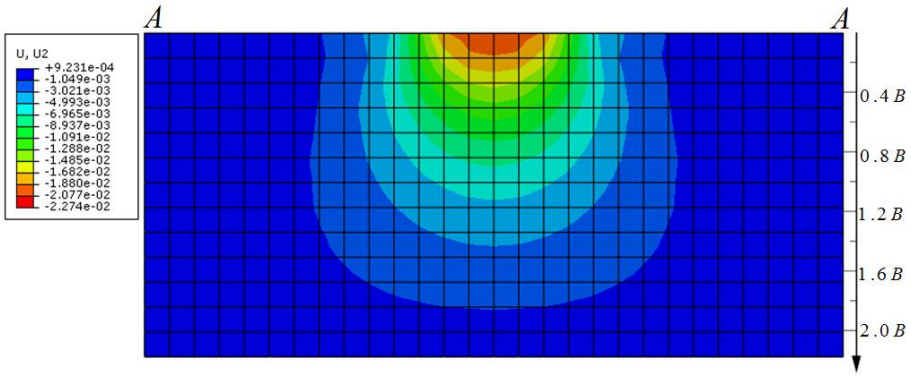


(a) Unreinforced sand bed

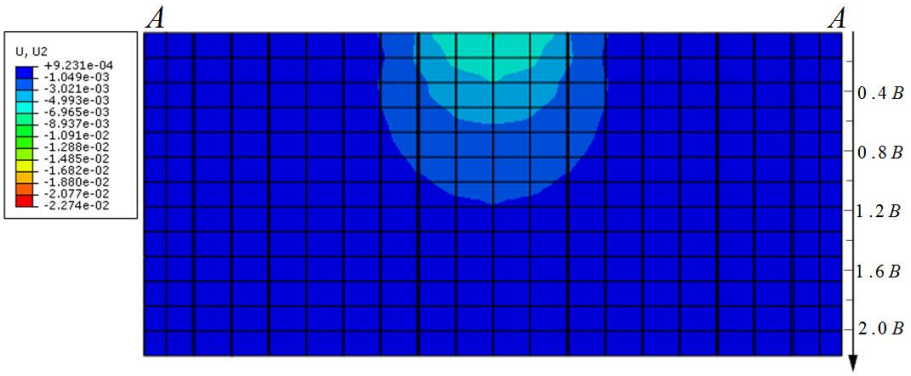


(b) Geocell reinforced sand bed

Fig. 4. Contours of vertical displacement for different cases ($p$= 300kPa, "A" cross section)

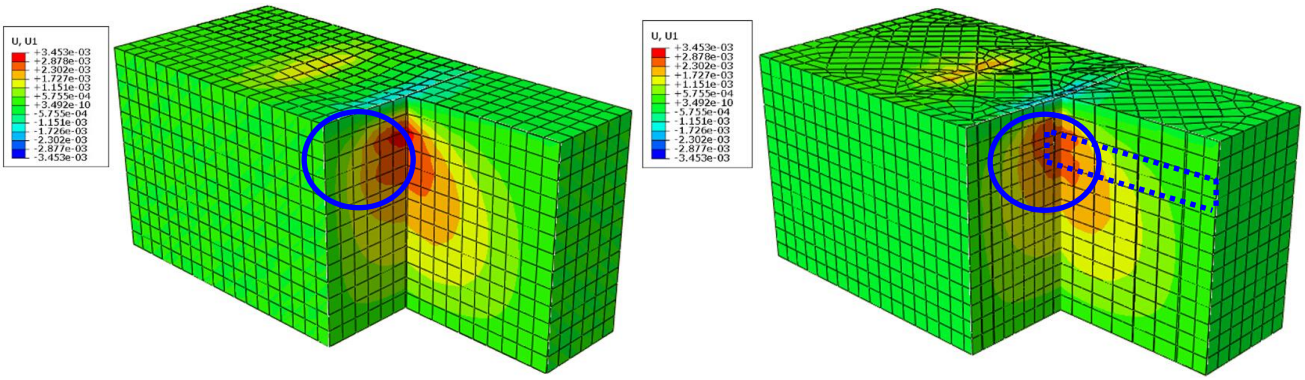


(a) Unreinforced sand bed (b) Geocell reinforced sand bed

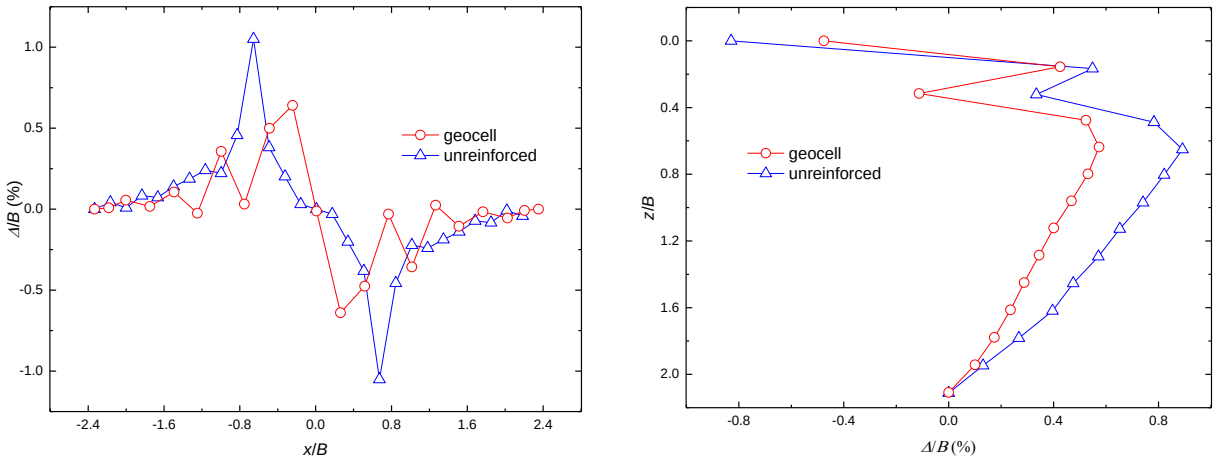


(c) Comparison of different cases ($x$ direction) (d) Comparison of different cases ($y$ direction)

Fig. 5. Contours of horizontal displacement for different cases ($p$= 300kPa, "A" cross section)

also can be seen that the depth is 0.3*B* and 0.5*B* in unreinforced and geocell reinforced case respectively when the max horizontal displacement is reached. This reveals that as compare to the unreinforced sand bed, geocell showed better attenuation of the horizontal displacement under the center of footing which in turn avoid the local failure of the sand. Chung and Cascante (2007) also have shown that a zone between 0.3*B* and 0.5*B* is identified to maximize the benefits of soil reinforcement. They noticed that the accommodation of reinforcements within one footing width below the foundation can lead to an increase in bearing capacity. However, in LEIG geocell reinforced sand bed, it can be seen that the influence zone extend around 2*B*. This might imply that the higher the stiffness of geocell is the depth the influence zone is.

Fig. 6 shows the horizontal displacement contours of "B" cross section for different cases. Comparing the Fig.6 to Fig. 5, it can be found that the horizontal displacement of the reinforced foundation bed prominently decreased as compared to the unreinforced one. The confinement of the all-round of geocell can be obviously in 3-dimention.

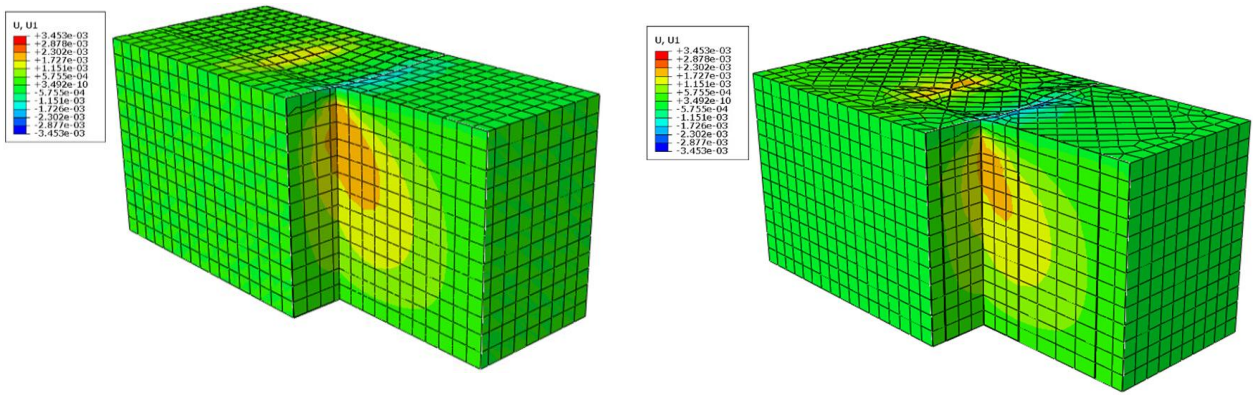


(a) Unreinforced foundation (b) Geocell reinforced foundation

Fig 6 Contours of horizontal displacement for different cases (*p*= 300kPa, "B" cross section)

### 3.3 *Stress distribution*

The comparison of typical plots of stress distribution (*p*=300kPa) in the soil foundation was presented in Fig. 7. For both cases i.e., unreinforced and reinforced, the stress values reduce gradually away from the footing indicating that failure is progressive. The contour interval is narrower in Fig. 7b than in Fig. 7a indicates that the stresses are more uniform in the geocell reinforced soil. This phenomenon tends to be more obvious with the development of the depth. Stresses were found to be distributed to the wider areas in the lateral direction and to the shallower in the vertical direction. Similar types of observations were also made by Hedge et al (2014b). Fig. 7c presents the comparison of vertical stresses at the depth of 0.5*B* (measured below the geocells). From Fig. 7c, it can be seen that the peak of stress in reinforced situation with geocell layer decreases about 33% comparing to unreinforced situation. From these observations it could be determined that due to the height of the geocell, the confinement of the all-round of geocell increases the stiffness of the reinforced base. As the geocell reinforced section is stiffer than the surrounding soil, the curved surface exerts upward reaction and reduces the net stress applied to the subgrade. The geocell mattress transfers the footing load to a deeper depth through the geocell layer. The reinforced layer acts like a stiff matt as a secondary footing and redistributes the footing load over a larger area and uniformly over the subgrade soil. In other words, the geocell reinforced mattress provides a stronger plate effect and resulted in reducing the vertical stress compared to the unreinforced soil.

### 3.4 *Stress distribution on the surface of geocell*

The tensile stress distribution on the surface of geocells was presented in Fig. 8. From Fig. 8a, it can be seen clearly that the tensile stress is more concentrated in the median cell which directly below the footing. The tensile stress tends to reduce gradually away from the median cell. It confirmed that the tensile stress in the region under the footing is substantially high compared to that in the region outside the loaded area as indicated in Fig. 5 and Fig. 7. Variations of the tensile stress on the strip of the geocell (which is lined out in dash line on the Fig. 8a) are depicted in Fig. 8b. The distance between two adjacent displacement joints of geocell is 20cm, the total length of strip is 160cm. From the Fig. 8b, it could be observed that the plot was framed with something like wave "~" between two adjacent joints. This revealed that the part of strips adjacent to the joints of geocell is easiest to be destroyed which can be confirmed by

the results of model test (Han et al. 2014) and a cell simulation (Hou et al. 2015). It also can be found that the tensile stress tends to be vanished when the distance from the center of the footing is greater than 1.5*B*. This confirmed that the length of geocell layer has an optimum value, beyond which further improvements were marginal.

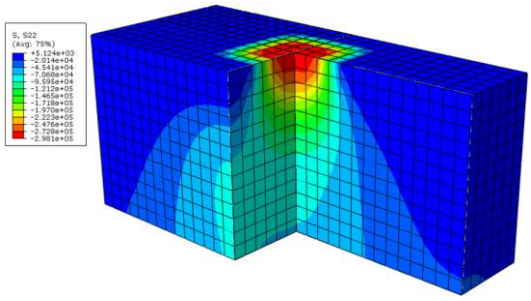

Unreinforced soil foundation

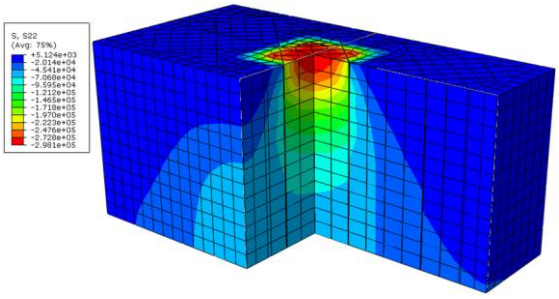

(b) Geocell reinforced soil foundation

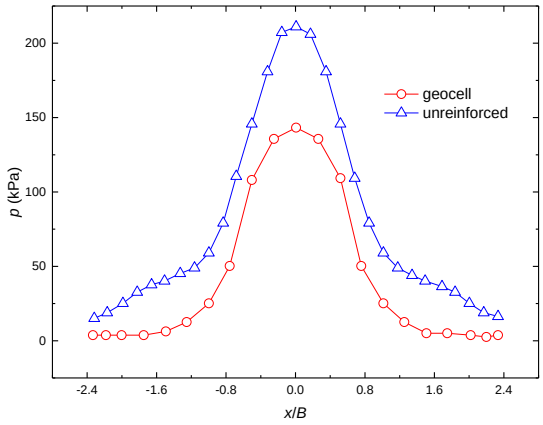


(a) Comparison of different cases

Fig 7 Stress distribution ($p$=300kPa, "A" cross section)

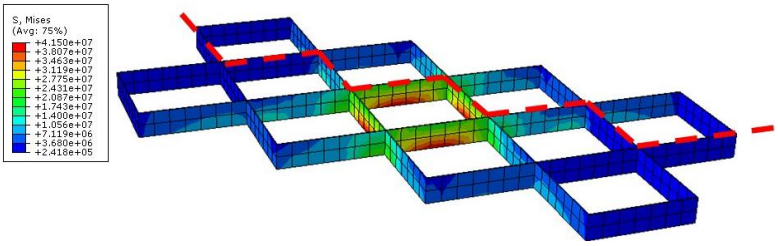


(a) Tensile stress on the geocells

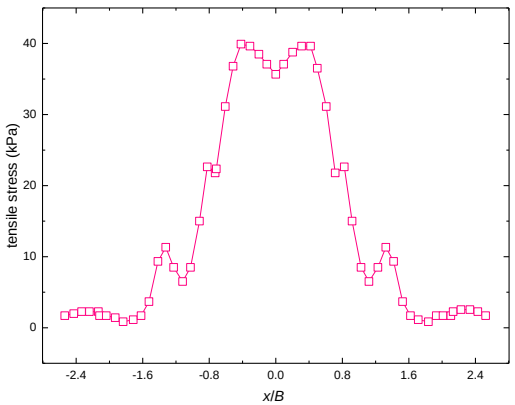


(b) Tensile stress on a strip

Fig 8 Tensile stress distribution on the surface of geocells

## 4 CONCLUSION

3-D finite-element analyses were conducted using ABAQUS software package to investigate the effect of a new lock enhanced integral geocell on the response of soil foundation. Some of the conclusions inferred from the results are as follows:

(1) In case of geocell, the vertical displacement is more uniform and can be transferred to a relatively shallow depth as compared to the unreinforced one.

(2) The geocell reinforced case yields the more uniform reduction of horizontal displacement peaks than the unreinforced one. As compared to the unreinforced sand bed, geocell showed better attenuation of the horizontal displacement under the center of footing which in turn avoid the local failure of the sand and increase the bearing capacity.

(3) Stresses were found to be distributed to the wider areas in the lateral direction and to the shallower in the vertical direction in geocell reinforced base.

(4) The tensile stress is more concentrated in the median cell which directly below the footing. The maximum contact stress can be found at the top of four joints of cell which is under the footing.

(5) The geocell-reinforced base can provide lateral and vertical confinement, tensioned membrane effect, and wider stress distribution and result in increasing the bearing capacity and reduce the settlement.

## ACKNOWLEDGMENTS

This study has been supported by the National Natural Science Foundation of China (NSFC) (No. 41372280 & 41202215). The authors would like to express their gratitude for these financial assistances.

## REFERENCES

Bathurst R.J., Nernheim A,Walters D.L., Allen T.M., Burgess P, Saunders D.D. 2009. Influence of reinforcement stiffness and compaction on the performance of four geosynthetic-reinforced soil walls. Geosynth Int, Vol. 16(1), pp. 43-49.

Chung W and Cascante G. 2007. Experimental and numerical study of soil reinforcement effects on the low-strain stiffness and bearing capacity of shallow foundations. J Geotech Geoenviron, Vol. 25(3), pp. 265-281.

Dash SK. 2012. Effect of geocell type on load-carrying mechanisms of geocell-reinforced sand foundations. Int J Geomech, Vol.12(5), pp. 537-548.

Han J, Yang X, Leshchinsky D, Parsons R.L. 2007. Behavior of geocell reinforced sand under a vertical load. J Transp Res, Vol. 2045, pp. 95-101.

Han X, Zhang M.X., Li J.Y., Jiang S.W. 2014. Model test of sand foundation reinforced with high-strength geocell. J Yangtze River (in Chinese), Vol. 31(3), pp. 27-33.

Hegde A, Sitharam T.G. 2014a. 3-Dimensional numerical modelling of geocell reinforced sand beds. Geotext Geomembr, Vol.43(2), pp. 171-181.

Hegde, A.M., Sitharam, T.G. 2014b. Effect of infill materials on the performance of geocell reinforced soft clay beds. Geomech Geoengin, Vol. 7, pp. 1-11.

Hou J, Zhang M.X., Han X, Li R. 2015. Mechanism of a high-strength geocell using FEM. J Geotech Eng (in Chinese), Vol. 7, pp. 26-30.

Latha G.M., Dash S.K., Rajagopa K. 2014. Numerical simulation of the behavior of geocell reinforced sand in foundations. Int J Geomech, Vol. 9(4), pp. 143-152.

Lee J & Eun J. 2009. Estimation of bearing capacity for multiple footings in sand. Comput. Geotech, Vol. 36(6), pp. 1000-1008.

Leshchinsky B and Ling H.I. 2013. Numerical modeling of behavior of railway ballasted structure with geocell confinement. Geotext Geomembr, vol. 36(1), pp. 33-43.

Mehdipour, I, Ghazavi, M, Moayed, R.Z. 2013. Numerical study on stability analysis of geocell reinforced slopes by considering the bending effect. Geotext Geomembr, Vol. 37, pp. 23-34.

Q/DK02. 2011. The new standards for geocell in China.

Yuu, J., Han, J., Rosen, A. 2008. Parsons, RL., Leshchinsky, D. Technical review of geocell-reinforced base courses over weak subgrade. The first pan American geosynthetics conference & exhibition proceedings. Appendix VII, Cancun, Mexico,

Zhou, H. & Wen, X. 2008. Model studies on geogrid or geocell reinforced sand cushion on soft soil. Geotextiles Geomembr, Vol. 26(3), pp.231-238.